1 **Title: Behavior of Rare Earth Elements in an Aquifer Perturbed by CO_2 Injection : Environmental**

2 **Implications**

3 **Highlights**

4 • The behavior of dissolved REY in groundwater within the critical zone is difficult to evaluate

5 • Behavior of REY and trace metals was studied upon an aquifer perturbated by CO_2 injection

6 • A geochemical model was used to evaluated dissolved REY behavior

7 • REE complexation is/are the main factors controlling REE release and fractionation

8 • REY fractionation can be used to predict bulk water-rock interaction

9 **Authors : Jean Rillard[1], Olivier Pourret[2], Paolo Censi[3], Claudio Inguaggiato[4], Pierpaolo Zuddas[5],**

10 **Pierre Toulhoat[6], Philippe Gombert[7], Lorenzo Brusca[8]**

11 [1] BRGM, 5 rue de la Goelette 86280, Saint Benoit, France

12 [2] UniLaSalle, AGHYLE, 19 rue Pierre Waguet, 60026 Beauvais, France

13 [3] Department of Earth and Marine Sciences, University of Palermo, Via Archirafi, 36, 90123 Palermo,

14 Italy

15 [4] Departamento de Geología, Centro de Investigación Científica y de Educación Superior de Ensenada

16 (CICESE), Carretera Ensenada-Tijuana 3918, Ensenada, Baja California, México

17 [5] Sorbonne Universités, UPMC Univ. Paris 06, CNRS ISTEP, 4 place Jussieu, 75005 Paris, France

18 [6] BRGM, 3 av. Claude Guillemin 45060 Orléans, France

19 [7] INERIS, Parc Technologique Alata, 60550 Verneuil-en-Halatte, France

20 [8] INGV National Institute of Geophisics and Volcanology, Section of Palermo, Via U. La Malfa, 153,

21 90146 Palermo, Italy

22

26

Abstract

Three cubic-meters of CO_2-saturated water was injected into a subsurface fractured aquifer in a post-mined area, using a push-pull test protocol. Groundwater samples were collected before and after CO_2-injection to quantify geochemical changes. CO_2-injection initially reduced the pH of water from 7.3 to 5.7, led to the enrichment of major ions (Ca^{2+}, Mg^{2+}, and alkalinity), and dissolved trace metals (including Fe, Mn, As, and Zn) in the groundwater. Rare earth elements (REE) and yttrium concentrations were also measured in these samples before and after CO_2 perturbation, to evaluate their behavior. An enrichment of total Y plus REE (REY) occurred. REY fractionation was observed with higher heavy REE (HREE) enrichment compared to light REE (LREE), and significant variations in La/Yb and Y/Ho ratios were observed following CO_2 perturbation. Enrichment by a factor of three was observed for Y, Lu, and Tm, and by nearly one order of magnitude for Dy and Yb. A geochemical model was used to evaluate the amount of REE aqueous ions complexed throughout the experiment. Modeling of the results showed that speciation of dissolved REE with carbonate, along with desorption from iron oxyhydroxide surface were the main factors controlling REE behavior. This study increases an understanding of dissolved REE behavior in the environment, and the potential use for applying iron oxides for REE recovery from mine drainages. Furthermore, the description of REE fractionation patterns may assist in surveying CO_2 geological storage sites, surveying underground waste disposal sites, and for understanding the formation of ore deposits and fluid inclusions in geological formations.

Introduction

The behavior of rare earth elements (REEs) in natural environments has been extensively studied (Michard 1989; Johannesson et al. 1995, 1997; Choi et al. 2009; Noack et al. 2014). REEs are valuable as components in electronic and renewable energy technologies. The European Community classifies REEs as critical raw materials (European Community, 2010, 2017).

An understanding of REE mobility, their accumulation, and their global cycling mechanisms in the natural environment, is important for evaluating their reserves for future use (Pourret and Tuduri 2017), and to anticipate environmental issues involved in the intensive exploitation of these materials (Filho 2016; Edahbi et al. 2018a).

Extraction of REEs and associated critical elements have been optimized using in-situ leaching techniques to enhance their extraction rates (Haschke et al. 2016; Vahidi et al. 2016). Dissolved REE fractionation patterns have been used as a proxy for understanding many geodynamic processes, such as magmatic melting and water-rock interactions (Bau 1996, 1999; Irber 1999). Dissolved REE studies also suggest methods for tracing the environmental impacts of human activity, including

60   shale gas hydraulic fracturing fluid analysis (Yang et al. 2018). The physico-chemical properties of

61   REEs allow them to be used as robust proxies for studying low and high-temperature geochemical

62   reactions (Pérez-López et al. 2010; Hannigan and Sholkovitz 2001).

63   The geological storage of CO_2, which is part of carbon capture and storage (CCS) technology, has

64   been considered a potential method for reducing the accumulation of atmospheric greenhouse gases

65   (IPCC 2005). Geological storage involves injecting CO_2 previously captured from industrial processes

66   into deep underground rock formations. The aim of doing so is to permanently remove CO_2 from the

67   atmosphere. The effectiveness of storage depends on the reservoir storage site's capacity and

68   integrity. CO_2 storage capacity is driven by porosity, reservoir permeability, and the existence of a

69   sufficient impermeable barrier or cap rock for containing the CO_2 permanently. Several types of

70   geological formations have been identified as having a suitable capacity for CCS. To date, these

71   reservoirs include deep saline aquifers, coal bed formations, oil and gas reservoirs exploited through

72   enhanced oil recovery technics using CO_2, and finally, depleted oil and gas reservoirs. Among these

73   storage sites, deep saline aquifers have been identified for having larger storage capacity and

74   worldwide distribution (see Bachu et al. 2007 and global references on the website

75   www.globalccsinstitute.com).

76   Once injected, part of the CO_2 will be physically trapped beneath the impermeable cap rock, which

77   acts as a seal, and the remaining CO_2 will dissolve into the aqueous phase. Part of this dissolved CO_2

78   may react with reservoir rocks to form a new mineral (CO_2 mineral trapping), or alternatively, may

79   remain dissolved into the aqueous phase (solution trapping) (Bachu et al. 1994). As such, an

80   understanding of CO_2-water-rock interaction processes are of primary importance for validating the

81   feasibility and effectiveness of CCS. To study this phenomenon, numerous experiments have been

82   performed under laboratory conditions alongside geochemical models (Little and Jackson 2010; Liu

83   et al. 2012; Humez et al. 2013; Pearce et al. 2015). Modeling of experimental data offers accuracy for

84   chemical reaction descriptions, but is fairly limited in terms of time and scale. The study of natural

85   CO_2-rich hydrothermal water offers good analogues for studying long-time CO_2-water-rock

86   interaction, but appears limited in its ability to describe chemical phenomena with a good degree of

87   precision (Gilfillan et al. 2009; Keating et al. 2010; Gal et al. 2012). Several field experiments have

88   been performed as pilot tests for identifying the scale of CCS sites, and to identify technical and

89   scientific gaps (see Jenkins et al. 2015, and references therein).

90   The above-noted experimental works have shown that several issues must be resolved, including the

91   environmental risks involved in CCS processes. Several preliminary experiments, in the field and in

92   the laboratory, suggest the potential risks of releasing dissolved trace metals into subsurface

93   freshwater aquifers. The release of dissolved metals may be caused by CO_2-enriched brine leaking

94   from an initial deep storage reservoir, and moving toward the surface. Among other phenomena, the

95   remobilization of trace metals is related to in-situ pH and redox perturbations involved in CO_2-

96   injection or leakage. In particular, CO_2 perturbation may involve pH acidification, thereby enhancing

97   dissolution of the reservoir rock, and generating the release of trace metals that may initially be

98   present in the reservoir rock minerals, or that have been sorbed onto mineral surfaces (Kharaka et al.

99   2006; Little and Jackson 2010; Wilkin and Digiulio 2010; Siirila et al. 2012; Wunsch et al. 2013; Rillard

100 et al. 2014; Jenkins et al. 2015). Understanding the fate and transport of trace metal elements in

101 subsurface geological environments is therefore important. These issues are also valuable for other

102 geoengineering applications such as toxic waste disposal, long-term underground storage of

103 radioactive waste, and monitoring of waste landfills.

104 CO_2-water-rock interactions are driven by the crystallization of newly-formed minerals at the fluid-

105 rock interface. Thus, the feasibility of CO_2 storage is based on a surface-driven process and elements

106 of the lanthanide series which, along with yttrium, represent a promising geochemical tool for

107 describing processes occurring at the interface between injected fluids and host rock. The behavior

108 of REY in groundwater may help to understand the reactions occurring at the water-rock interfaces

109 following interaction with injected CO_2.

110 Shand et al. (2005) highlight that the concentration of dissolved REE in groundwater is controlled by

111 several factors. These include the release of chemical elements resulting from weathering processes,

112 groundwater pH and redox reactions, adsorption processes, complexing ligands in groundwater, and

113 physical hydrogeological factors (hydrodynamic processes and residence time). Studies of dissolved

114 REE behavior within geothermal fluids and natural CO_2-rich water sources have produced useful

115 results. A fractionation pattern for REEs occurs during CO_2, water, and rock interaction processes, and

116 a strong relationship has been identified between dissolved REEs and water pH (Lewis et al. 1998;

117 Michard 1989; Shand et al. 2005; Inguaggiato et al. 2015). The use of REEs as tracers of high salinity

118 brine leakage detection in CCS applications has been studied under laboratory conditions (McLing et

119 al. 2014). However, several issues were presented, such as the high salinity content of samples,

120 which caused analytical problems for trace metal analyses.

121 REE signatures in fluid inclusions is also a key parameter for enhancing an understanding of the

122 behavior of deep geological fluids. In particular, REE fractionation patterns are good proxies for

123 evaluating the physico-chemical conditions, fluid-mixing, and precipitation processes operating

124 during the genesis of valuable geological resources, such as oil, gas, and ore deposits (Zwahlen et al.

125 2019; Shu and Liu 2019; Perry and Gysi 2018).

During mineral crystallization, REEs behave as a function of their ionic charge and radius (charge and radius controlled (CHARAC) processes; see Bau 1996). During aqueous processes, however, these metal cations react based on their external electronic configuration. As such, the main change in the features of normalized REE concentrations, and in the Y/Ho ratio, can be recognized through interactions at the rock-fluid interface (Bau et al. 1998, 2003; Irber 1999; Negrel et al. 2000; Takahashi et al. 2002). Of special importance is the scavenging of REEs by metallic oxide and hydroxide phases (i.e. oxyhydroxides such as iron and manganese oxyhydroxides), which affects REEs species in aqueous media (De Carlo et al. 1998; Quinn et al. 2006; Schijf and Marshaal 2011; Liu et al. 2017). Complexation of REEs onto iron and manganese oxides is strongly pH-dependent (Bau 1999; Verplanck et al. 2004; Quinn et al. 2006, 2007). The binding of these cations to an amorphous phase such as ferrihydrite (e.g. $Fe(OH)_3$) is important, due to the large reactive surface area of these minerals. Using zerovalent iron nanoparticles for REE recovery from acid mine drainage under laboratory conditions showed the ability of these oxyhydroxide minerals to remove REEs from a solution (Crane and Sapsford 2018). Fractionation between light REEs (LREEs) and heavy REEs (HREEs) occurs during scavenging onto metal oxides. This is primarily driven by dissolved species complexation, particularly in the presence of carbonate species (De Carlo et al. 1998; Bau 1999; Ohta and Kawabe 2001; Quinn et al. 2007; Schijf and Marshall 2011; Munemoto et al. 2015). Many studies have evaluated REE complexation with organic and inorganic ligands. The complexation process of REEs occurring on mineral or organic surfaces is key to understanding the behavior of dissolved REE patterns in the environment (Wood 1990; Tang and Johannesson 2003; Pourret et al. 2007; Pourret and Martinez 2009; Pourret et al. 2010).

Understanding dissolved REEs' behavior is challenging, due to the involvement and interdependence of the phenomena described above. The aim of this experimental work is to study the potential enrichment of dissolved trace metals and REY in groundwater perturbated by CO_2, and its potential application to CO_2 geological storage safety site assessment. An existing study employing this experiment focused on major chemical elements and trace metal remobilization for studying the potential environmental issues involved in CCS (Rillard et al. 2014). A second set of samples, collected during the same fieldwork, was used to study the behavior of dissolved REE. The aim of the present study is to quantify the effect of CO_2 and pH-perturbation of the aquifer on release of dissolved REY. This work may enhance an understanding of the fate and transport of dissolved REEs and associated trace metals into the environment, for evaluating the safety of geological CO_2 storage. The results may also be useful for other geoengineering applications, including the geological storage of radioactive waste and mine site remediation.

1. Geological and hydrogeological site setting

The detailed geological and hydrogeological settings of the experimental site is described in Rillard et al. (2014). The experimental site is located in the Lodève area, Southern France, roughly 80 km north of Montpellier. The local geology involves large Permian sandstones and shales lying on top of Cambrian dolomites. Sandstones are dark-red in color, due to high concentrations of iron hydroxides, while shales are characterized by grey coloring, due to their high organic matter content. The experiment site is situated within a 400 meters-thick sandstone and shale formation. From the 1950s to the early 1990s, this area had been extensively mined for uranium and arsenic using underground galleries and open pit mines, due to the high concentration of trace metals in the bedrock.

Denser mineralized deposits representing higher concentrations of metals can be found in vein deposits throughout the fractured network. The mineralization processes have been attributed to hydrothermal fluid circulation and associated secondary mineral precipitation (Brockamp and Clauer 2013; Laurent et al. 2017). The primary mineralogical association between arsenic and uranium refers to arsenuranospathite deposits (Dal Bo et al. 2015). This area is also characterized by hydrothermal activity, with hot springs that are sometimes naturally enriched with CO_2, and locally exploited for geothermal energy (Bonnaveira et al. 1999).

The sandstone and shale formations are characterized by low permeability (estimated by a pumping test at 10^{-7} m.s^{-1}) and low total porosity (estimated at less than 5%). Groundwater circulation mainly occurs via a network of rock fractures.

The following average modal composition of major minerals in the host-rock was determined: dolomite (20%), albite (20%), K-feldspar (30%), quartz (15%), illite (10%), other (5% calcite and iron oxihydroxide, siderite, and pyrite) (Brockamp and Clauer 2013; Chopin 2016). However, mineral compositions may vary among different strata. Indeed, significant amounts of neoformed mineral phases were observed along the surface fractures by camera logging, performed immediately after experimental well implementation. In particular, the presence of amorphous iron oxihydroxides was identified as a product of pyrite oxidation (Rillard et al. 2014).

2. Materials and methods

A field experiment using a CO_2-rich water injection was performed following a push-pull test protocol (Haggerty et al. 1998; Istok et al. 1997; Matter et al. 2007). This experiment configuration offered an intermediate scale between laboratory experiments, where chemical reactions can be constrained and accurately described, and larger scale studies in natural CO_2 hydrothermal fields. In the latter,

the CO_2 quantity involved and the hydrodynamic processes (mixing, residence time, etc.) is difficult to quantify. A 115 meters-deep well was drilled through the sandstone and shale formations. The well was cemented and equipped with PVC tubing on the uppermost 20 meters, in order to avoid contamination from surface and subsurface water. No equipment (or tubing) was installed from 20 meters to 115 meters deep in order to avoid contamination by well-tubing alteration, as shown in previous works (Kharaka et al. 2006). The entire geological well-log is presented in Rillard et al. (2014). Several hydrogeological prospections (pumping tests, packer test, microflow logging, tracing test, well-logging, physicochemical groundwater logging) were performed to determine the most suitable depth interval for injecting CO_2- saturated water. The injection was performed along a 3 meters interval located at a 56 meters depth within a fractured zone, through the sandstone layer. This injection zone was isolated using a double-packer system.

A 3 m^3 volume of baseline groundwater was initially pumped from the isolated well interval, temporarily stored in a water tank, and then saturated with pure CO_2 using a bubbling system. Once CO_2-saturation was reached (determined by a stable pH of 5.7, from an initial value of 7.3), the 3 m^3 volume was injected through the packer system, following a single-well push-pull test protocol (Haggerty et al. 1998; Istok et al. 1997; Matter et al. 2007). Samples were collected from the water tank before and after CO_2-saturation in order to determine baseline groundwater composition. An elapsed time of 80 hours was employed following the injection phase, to provide a sufficient interaction time between the injected solution and the host rock. This 'interaction' time was followed by a 80 hours pumping period at 0.5 m^3/h debit to re-pump the 3 m^3 injected volume, plus the mixed-formation water. This protocol was adapted from studies by Haggerty et al. (1998), Istok et al. (1997), and Matter et al. (2007).

Samples were systematically collected over the entire pumping period to evaluate the impact of CO_2 perturbation on groundwater chemical composition. A sampling protocol using a glovebox and inert plastic bottles, previously filled with nitrogen gas, was used to minimize sample oxidation and contamination. Samples used for metal analysis were filtered in the field using a 0.2 μm filter, and acidified using HNO_3 Normapur (70%), until reaching a pH<2. A second set of samples was filtered in the field using a 0.45 μm filter for major cations and anions analysis. Physicochemical parameters, pH, conductivity, temperature, and redox potential were continuously monitored using a flow-through cell, installed at the top of the well during the injection and pumping phase. Fe (II) was measured in the field for individual samples collected, using a portable spectrophotometer-specific IRON(II) LR® reagent. Alkalinity was measured in the field by HNO_3 acid titration of regularly-collected individual samples.

225   A list of the samples used for specific REE analyses is presented in Table 1. The corresponding pH,

226   redox potential, and conductivity measured in the field, and the ratio of pumped volume divided by

227   injected volume illustrates the pumping stage evolution corresponding to each individual sample.

228   Samples 1 to 19 were collected at different intervals during the pumping phase. Sample 1 was

229   collected a few minutes after the start of pumping. Sample 19 was collected roughly 24 hours after

230   the start of pumping.

231

232

233   The analysis for REEs and several additional trace elements was performed at the Istituto Nazionale

234   di Geofisica e Vulcanologia (INGV) geochemical laboratory in Palermo, Italy. REEs were analyzed by

235   Q-ICP-MS (Agilent 7500ce). A mass spectrometer was calibrated in the range of 5-5000 ng/L, with 11

236   calibration points obtained by stepwise dilution of a REE multi-element standard solution. The

237   sensitivity variations were monitored using internal standards [103]Rh, [115]In, and [185]Re, mixed into the

238   sample before the nebulizer device. A 60 seconds rinse using a 2% HNO_3 solution and 0.5% HCl

239   solution, plus a 60 secondes rinse using a 2% HNO_3 solution reduced memory interferences between

240   samples. Standards and samples were replicated five times to evaluate the data precision by relative

241   standard deviation (RSD), which was always <15%. The standard reference materials SLRS4

242   (Lawrence et al. 2006), and SpectraPure Standards SW1 and SW2 were analyzed to evaluate data

243   accuracy, which never exceeded 10%.

244

245   **3. Speciation model with PHREEQC**

246   To understand the parameters controlling REE behavior as a result of CO_2-injection, a geochemical

247   model was used, with particular attention paid to sorption/desorption processes and speciation

248   phenomena.

249   The speciation modeling for Fe-oxide equilibrium calculations was achieved using hydrogeochemical

250   code PHREEQC ver. 3.3.9 (Parkhurst and Appelo 2013), as well as the wateq4f database. This

251   database was updated using the well-accepted stability constants for the 14 naturally occurring REEs

252   at zero ionic strength, and at 25°C. These constants account for inorganic aqueous complexes with

253   carbonate, hydroxyl, sulfate, chloride, and fluoride anions. The stability constants for $LnCl^{2+}$ and

254    $LnCl_2^+$ were taken from Luo and Byrne (2001), and LnF^{2+} and LnF_2^+ were taken from Luo and Millero

255   (2004). Those for $LnSO_4^+$ were obtained from Schijf and Byrne (2004), and those for $LnNO_3^{2+}$ from

256   Millero (1992). Constants for $Ln(OH)^{2+}$ and $Ln(OH)_2^+$ were taken from Lee and Byrne (1992), and those

257   for Ln(OH)$_3$(a) from Klungness and Byrne (2000), respectively. Equilibrium constants for the
258   formation of LnCO$_3^+$ and Ln(CO$_3$)$_2^-$ were taken from Luo and Byrne (2001). Scavenging model
259   parameters for HFO were taken from Liu et al. (2017). Precipitation of HFO was quantified from
260   dissolved Fe measured in groundwater samples, and the corresponding equilibrium constants were
261   taken from Nordstrom et al. (1990). The number of REE binding sites in the reactive solid surfaces
262   was determined by the moles of HFO, precipitated and defined explicitly by the keyword data block
263   'EQUILIBRIUM PHASES'. The specific surface area (SSA) was defined relative to the moles of HFO, in
264   which the amount of specified binding sites changed as the SSA varied during the batch-reaction
265   simulation. Upon HFO formation, the two types of oxide surface binding sites (= S^{s}OH and = S^{w}OH)
266   were assumed to be available for REE complexation. For surface complexation modeling, both the
267   surface-bound and diffuse layer species were taken as components of the system in the presence of
268   iron oxyhydroxides. In this modeling configuration, iron hydroxides were only considered as solid
269   phase (i.e., colloid or mineral phase).

270   All of the REEs considered in the model were trivalent, and followed the hypothesis of Bau (1999)
271   that oxidation-scavenging of Ce by metal oxides included three independent steps: (1) sorption of
272   Ce(III) from solution; (2) partial oxidation of Ce(III) to Ce(IV) on the iron or manganese oxide surface;
273   (3) partial desorption of Ce(IV) to solution.

274   **4. Results**

275   **4.1 REY enrichment and fractionation following CO$_2$ perturbation**

276   The physicochemical parameters (pH, redox, and conductivity) measured in the field during the
277   experiment are listed in Table 1 and represented in Fig. 1 as functions of the ratio of pumped volume
278   to injected volume (i.e. Vp./Vinj.). The evolution of iron and manganese, as major reactive metals
279   following the CO$_2$-injection, is represented in Fig.2a. Other parameters that may influence REY
280   behavior such as aluminum content did not show clear evolution following CO$_2$ perturbation.
281   Dissolved organic carbon (DOC), as well as total organic carbon (TOC), were below the detection limit
282   for all the samples. A clear increase for As and Zn was correlated with CO$_2$ perturbation. The specific
283   behavior of these elements, as well as other major parameters (Ca^{2+}, Mg^{2+}; alkalinity, etc.) are
284   presented in detail in Rillard et al. (2014). Only parameters that have been identified as having an
285   impact on REY behavior were studied in the present paper.

286

287   In this study, the entire REEs series plus Y was analyzed. A small number of representative elements
288   per group of REEs is presented in molar concentration as a function of Vp./Vinj ratio (see Fig.3): Ce

289   for the LREE group, Gd and Dy for MREE, and Yb and Y for HREE. A Vp./Vinj. ratio close to zero

290   represents the beginning of the pumping stage, and the most CO_2-perturbed sample. A global

291   enrichment in REY concentration was observed following CO_2-injection (Fig.3). The ∑REY increased

292   from $1.2 \cdot 10^{-9}$ mol/L to $4.3 \cdot 10^{-9}$ mol/L, following a pH decrease (Fig.4). Higher enrichment was

293   observed for Y (from $8.1 \cdot 10^{-10}$ mol·L^{-1} to $3.2 \cdot 10^{-9}$ mol·L^{-1}) (Fig.3, Y image). Global REE enrichment

294   following CO_2 perturbation was induced by acidification related to carbonic acid production.

295   Acidification enhanced host rock mineral weathering, releasing trace metals into the aqueous phase.

296   Global REY enrichment mimics the global increase in dissolved metals, such as iron and manganese

297   (see Fig.2, and Rillard et al. 2014). This was evident when comparing the baseline groundwater

298   composition (baseline groundwater sample) to the most perturbed CO_2 sample (Sample 1). However,

299   the enrichment was not homogeneous along the entire REEs spectrum. Enrichment in dissolved REEs

300   and global correlation with CO_2 perturbation appeared greater for Y and HREE (Fig.3). Good

301   correspondence between dissolved concentration and CO_2 perturbation was observed for Y, Dy, Er,

302   Tm, Yb, Lu, Gd, and Tb (i.e. MREE and HREE). A regular increase in the concentration of ∑HREE (plus

303   Y) occurred alongside a pH decrease, as a result of CO_2 perturbation, until the end of the pumping

304   phase, as shown in Fig. 4. The increase in MREE appeared less-marked as a function of pH and

305   Vp./Vinj (Fig. 4). In contrast, no systematic evolution was observed for LREE as a function of pH and

306   Vp./Vinj.

307   Typical REE parameter (La/Yb, Ce/Ce*) evolution as a function of Vp./Vinj. is shown in Fig. 5. The

308   La/Yb ratio shows an abrupt decrease following CO_2-injection, and a smooth increase toward the

309   baseline water ratio after Vp/Vinj. reached 0.5. No clear evolution was apparent for Ce/Ce* as a

310   function of Vp/Vinj. A decrease in Ce anomaly appeared to have occurred immediately after CO_2-

311   injection, but no clear trend was observed as a function throughout the entire pumping phase. The

312   fractionation of HREE compared to LREE appeared quite clear and was also confirmed by the

313   evolution of La/Yb ratio as a function of Vp./Vinj. (Fig.5). The Eu/Eu* anomaly was not considered,

314   since interference with BaO during analysis was suspected (Shabani et al. 1992; Dulski 1994; Zwahlen

315   et al. 2019). Despite the absence of a clear correlation between Ba and Eu (see supplementary

316   materials), the ratio Eu/Ba was >4000, and this may have led to a false positive Eu signal.

317   The entire REE pattern of the experimental samples, normalized to PAAS (Post Archeen Australian

318   Shale), is shown in Fig.6a. In order to simplify the visual result, only the most representative

319   experimental samples are presented: baseline groundwater; Vp.Vinj. = 0, representing the most

320   perturbed sample; Vp./Vinj. = 0.033 was the second most perturbed sample; Vp./Vinj. = 1.489 was

321   representative of a sample collected at the end of the pumping phase. Data for Eu are not shown,

322   since interference with Ba was suspected, as discussed above. The REE pattern showed a net

323 enrichment of HREE in both the baseline groundwater composition (baseline groundwater sample),

324 following CO_2-injection. This trend did not change significantly due to CO_2 perturbation. However,

325 the fractionation of HREE was significant following CO_2 perturbation. For comparison, the entire REE

326 pattern normalized to PAAS for bulk rock samples analysis is also presented in Fig 6b. These samples

327 were collected on the same shale and sandstone formation as the experimental site in this study

328 (data issued by Chopin 2016). The normalized to PAAS concentration of the bulk rock shows a clear

329 enrichment of HREE compared to LREE, in correlation with the general trend of REE observed for

330 water samples. However, a weak MREE enrichment (particularly for Gd, Tb, and Dy), compared to

331 LREE was observed. This point was not clearly indicated in the water samples. However, the

332 amplitude of this enrichment in MREE concentration remained limited (lower than 0.2).

333 **4.2. REE speciation**

334 REE speciation calculation results are shown in Fig. 7. The baseline water plot represents the baseline

335 groundwater sample, while sample one, with the lowest pH, represents the earliest sample collected

336 following CO_2 perturbation. The total proportion of REE complexes (%Ln3+; %LnCO3+ (CO3)2;

337 %LnSO4; %LnHFO) are represented as a function of pH and Vp./Vinj. ratio (see Fig.8).

338 The dissolved REE-carbonate complex is indicated as the dominant species prior to CO_2 perturbation

339 (Fig. 7, baseline groundwater sample). The proportion of REE complexation with carbonate was

340 nearly homogenous along the entire REE pattern, with no particular fractionation effects. REEs

341 sorbed to iron oxyhydroxide (Fig.7, Ln-HFO) indicates the second highest proportion in baseline

342 groundwater composition. The proportion of Ln-HFO complex increased with atomic weight along

343 the REE series, with a higher proportion of HREE sorbed, compared to LREE, for all samples. The

344 proportion of REE-sulfate complexes (Ln-SO_4^+) appeared low compared to the proportion of

345 carbonate complexes. A similar observation was made for free REE ions (Ln^{3+}).

346 Following CO_2 perturbation (see Fig.7, sample 1, and Fig. 8), the REE-sulfate complex became the

347 dominant species, except for Tm, Yb and Lu, for which the REE-carbonate was the dominant species.

348 The proportion of Ln-SO_4 complex decreased regularly alongside REE atomic weight, and the opposite

349 trend was observed for REE-carbonate (see Fig. 7, sample one to sample 19). The REE-iron

350 oxyhydroxide complex (HFO) decreased following CO_2 perturbation; this is particularly significant

351 when comparing the baseline groundwater to sample one (Fig. 7). From sample one to sample 19,

352 the Ln-carbonate and Ln-HFO complex proportions increased, and REE-sulfate complex decreased as

353 CO_2 perturbation diminished (Fig. 7). However, the total concentration of sulfate in groundwater did

354 not change significantly following CO_2 perturbation. The baseline concentration in sulfate was

355 relatively high. The sulfate concentration stayed at the same order of magnitude over the entire

11

356 experiment (within 7 mol/L to $9 \cdot 10^{-3}$ mol/L; see Rillard et al. 2014). A weak variation in SO_4

357 concentration was, however, observed during the experiment, but was attributed to the mixing

358 process, in accordance with hydrogeological information observed in the field (Rillard et al. 2014).

359 The initial high amount of sulfate in baseline groundwater was attributed to mixing with local

360 groundwater contaminated by former mine activities in the area (influence of acid rock drainage,

361 sulfide mineral oxidation, etc.). Therefore, the higher proportion of Ln-SO_4 following CO_2

362 perturbation is related to the higher affinity of dissolved REEs for complexing with sulfate in acidic

363 conditions (Decree et al. 2015), but not to an increase in sulfate concentration induced by CO_2

364 perturbation.

365 Enrichment of dissolved REEs was greater for Y and HREE. This was clear when comparing the La/Sm

366 ratio normalized to PAAS (La/Sm)$_{N-PAAS}$, and the La/Yb)$_{N-PAAS}$ ratio (Fig.5). La/Sm and La/Yb ratios

367 decreased after CO_2-injection, due to the higher amounts of HREE and MREE released in the water,

368 compared to the LREE. Similarly, a large increase in the Yb/Gd ratio (from 0.54 to 2.23) was observed

369 following CO_2 perturbation.

370 **5. Discussion**

371 **5.1. Effects of CO_2 perturbation on REY enrichment**

372 CO_2 perturbation increased the concentration of major elements (e.g. Ca^{2+} and Mg^{2+}) by nearly 30%,

373 and alkalinity doubled (Rillard et al. 2014). The pH initially decreased from 7.3 to 5.7, dissolved Fe

374 rose from $2.15 \cdot 10^{-5}$ mol/L to $1.17 \cdot 10^{-4}$ mol/L, and Mn from $1.35 \cdot 10^{-6}$ mol/L to $5.01 \cdot 10^{-6}$ mol/L.

375 Significant increases in dissolved trace metals, mainly As and Zn, were also observed (Rillard et al.

376 2014). Redox perturbation throughout the experiment was evaluated by comparing redox potentials

377 measured by electrodes in the field, with those calculated from the Fe (II)/Fe (III) equilibrium. Redox

378 potential was controlled by iron oxyhydroxide equilibrium, but was weakly perturbed and nearly

379 constant throughout the entire experiment (Fig.1).

380 The main geochemical reactions are identified by the geochemical model. The release of major

381 elements was attributed to weak dissolution and equilibrium of major minerals composing the host

382 rock, particularly dolomite and calcite. The increase in dissolved Fe was attributed to dissolution of

383 amorphous iron oxyhydroxides such as ferrihydrite (Fig. 2b). A good correlation was identified

384 between the saturation index of ferryhidrite and the dissolved iron concentration (Fig.2b). This is also

385 in agreement with the high amount of neoformed iron oxyhydroxide phases observed during drilling

386 operations. The release of dissolved iron is therefore mainly attributed to ferryhidrite dissolution.

387 The enrichment in Mn arose from the dissolution of Mn-oxides, but the specific phase could not be

388 identified using the geochemical model. The enrichment of trace metals, particularly As, is associated

12

389 with the desorption or dissolution of iron oxyhydroxides. The major factor for the enrichment of

390 trace metals induced by CO_2 is considered to be the acidic pH, derived from carbonic acid production.

391 The perturbation of redox conditions was not considered to be significant (Rillard et al. 2014).

392 The Ce/Ce* did not show clear evolution as a function of Vp.Vinj. (Fig. 5). The global anomaly of Ce

393 for all samples appeared negative (Tostevin et al. 2016), and a weak decrease appeared to have

394 occurred immediately after CO_2-injection, but this is not clearly evidenced in other samples. A cerium

395 anomaly is known for being a good proxy of redox potential variation (Bau and Alexander 2009; Frei

396 et al. 2013; Tostevin et al. 2016). A decrease in cerium anomaly can corroborate an oxidative

397 perturbation. However, the redox potential did not change significantly throughout the entire

398 experiment. The redox potential increased from +130 mV in baseline groundwater to +187 mV

399 following CO_2-injection (Fig.1).

400 Fig.10 illustrates the Y/Ho molar ratio as a function of Vp./Vinj. ratio. The Y/Ho ratio increased from

401 57 in baseline groundwater composition to >100 following CO_2 perturbation, before decreasing to

402 <80 when the V p./Vinj. ratio reached 1. The Y/Ho signatures are known to present different

403 behaviors during interactions with Mn and Fe-oxyhydroxides (Bau, 1996, 1999). An increase in Y/Ho

404 ratio was observed following CO_2 perturbation. Such enrichment of Y with respect to Ho was also

405 observed in natural CO_2-rich fluid by Shand et al. (2005). This result, however, is not consistent with

406 the dissolution/desorption of Fe/Mn-oxyhydroxides as the main sources of dissolved REEs. These

407 solids generally preferentially adsorb Ho, relative to Y, during authigenic crystallization (Bau 1999;

408 Bau and Koschinsky 2009). Therefore, the observed Y/Ho variation suggests that another REE-

409 enriched source released REEs into groundwater. This other source may be the desorption of REEs

410 from organic-rich shale surfaces (Haley et al. 2004; Takahashi et al. 2010). Another hypothesis is the

411 dissolution of carbonates or minerals, which may act as a source of anomalous Y (Tostevin et al.

412 2016). This final hypothesis is consistent with the dissolution of carbonate minerals (such as calcite

413 and dolomite) previously identified as a primary source of Ca^{2+}, Mg^{2+}, and alkalinity release, following

414 CO_2-injection (Rillard et al. 2014).

415 The enrichment in HREE relative to PAAS, within the entire REE series, in both baseline water

416 composition and following CO_2 perturbation, are described in natural CO_2 rich water (Shand et al.

417 2005), and in volcanic hydrothermal water sources (Inguaggiato et al. 2015, 2016, 2017). These data

418 support the preferential enrichment of HREE during weathering processes induced by CO_2

419 perturbation. However, as suggested above, some issues regarding analytical precision may have

420 affected some of the results. Due to the very limited volume of water in collected samples (less than

421 10 mL) and technical limitations, a preconcentration step could not be performed prior to REY

422 analyses with ICPMS. Overall REE concentrations ranged from 1241 pmol/L to 4300 pmol/L. These

423 concentrations are beyond the values in which REE preconcentration and a matrix-free method of

424 analysis are essential. However, the large variation observed in shale-normalized patterns for some

425 samples (the baseline groundwater sample in particular) may have been due to a lack of precision

426 resulting from chemical analyses. However, this point does not affect the general trend observed for

427 each individual REY element over the entire CO_2-injection experiment, as shown in Fig.3 and Fig.4.

428

429 **5.2 Effects of speciation and surface complexation on REY behavior**

430 Bau (1999) and Verplanck et al. (2004) showed that neoformed iron oxyhydroxides have a higher

431 affinity for HREE scavenging compared to LREE. Therefore, the higher enrichment of HREE may be

432 related to easier dissolution of neoformed hydroxide minerals such as ferrihydrite, following CO_2

433 perturbation (see Fig. 2, and Rillard et al. 2014). This hypothesis is supported by speciation

434 calculations showing a rapid decrease in the proportion of the Ln-HFO surface complex following CO_2

435 perturbation (see Fig.7, baseline groundwater sample 1, and Fig.8). HREE enrichment is also

436 illustrated in Fig.11, which represents the La/Yb ratio as a function of dissolved Fe concentration. As

437 the pH decreased, enhanced protonation of ferric oxide surfaces occurred, reducing the proportion

438 of negatively charged groups able to complex REE (Bethke, 2007). The modeling configuration only

439 considered the surface complexation onto solid iron hydroxide phases, as calculated in equilibrium,

440 with dissolved iron measured in the samples (this included the colloid or mineral phase comprising

441 the host rock of the aquifer). This model did not take into account solution complexation with iron

442 oxides. Thus, the development of a specific model is needed to study solution complexes with

443 dissolved iron. However, iron is known to easily form large-size colloids in a solution that mainly

444 control REE sorption and speciation (Pourret al. 2007, 2010).

445

446 Crane and Sapsford (2018) studied the sorption and fractionation of REE ions with zerovalent iron

447 nanoparticles. The aim of their work was to test the potential of recovering the dissolved REEs

448 contained in an acidic rock drainage solution. Their results showed that HREE had a higher

449 concentration, and faster scavenging, on a neoformed iron oxyhydroxide surface, compared to LREE.

450 Differences in coordination numbers between LREEs and HREEs helped to explain this phenomenon.

451 The differences affected the hydration number, with the number of REE ions decreasing from nine

452 for LREEs to eight for HREEs, with a transition region between Sm to Gd (Wood, 1990). This higher

453 coordination number may therefore preferentially restrict the bulk diffusion of LREE compared to

454 HREE on sorption sites. However, the experimental conditions were significantly different in the work

455　　presented by Cran and Sapsford (2018), compared to the present study (use of zerovalent iron with

456　　larger pH variation and redox potential).

457

458　　Furthermore, the global proportion of Ln-carbonate complexes decreased between baseline water

459　　(baseline groundwater sample) and the most CO_2 perturbed sample (sample 1 in Fig.7 and Fig.8). This

460　　decrease was less marked for HREE, and similar results were reported by Sholkovitz (1995), Byrne

461　　and Sholkovitz (1996), De Carlo et al. (1998) and Bau (1996). The greater stability of HREE carbonate

462　　complexes compared to LREE carbonates may explain the preferential release of HREE in water

463　　under the experimental conditions of this study.

464　　Speciation calculations show that in the more acidic samples (samples 1, 2, and 3), REE complexes

465　　occurred mainly with sulfate ($LnSO_4^+$), along with a higher proportion of complexed LREE (Fig.7 and

466　　Fig.8). However, this phenomenon did not involve the obvious enrichment of dissolved LREE. The

467　　proportion of REE sulfate complexes may have been overestimated by the model calculation. A

468　　higher proportion of REE sulfate complexes under acidic conditions was observed by Decree et al.

469　　(2015) and Verplanck et al. (2004).

470

471　　This speciation model was constructed using the database on speciation constants of REEs available

472　　to date. While these constants are well-documented for REE speciation carbonate and iron oxide

473　　species, a lack of data remains for other constants dealing with REE speciation in the presence of

474　　manganese oxyhydroxides, which may play an important role in dissolved REE behavior (Pourret et

475　　al. 2007b; Pourret and Tuduri, 2017; Liu et al. 2017). However, this model was able to provide

476　　important information for studying REE complexation with iron oxyhydroxides in Fe-rich

477　　groundwater aquifer systems (Verplanck et al. 2004; Quinn et al. 2007; Liu et al. 2017). The

478　　complexation with organic molecules (such as humic substances) was not taken into account in this

479　　study, since the organic carbon concentration (TOC and DOC) of the samples was below the

480　　detection limit. However, organic matter is known to effect important control on REE behavior

481　　(Pourret 2007a, 2007b, 2009). Further developments in modeling techniques should incorporate Mn-

482　　oxides, organic humic substances, and Fe-oxides simultaneously in a model, in order to better

483　　understand the roles of particle colloids in REE mobility in natural systems (Liu et al. 2017).

484

485　　**5.3 Tetrad effect**

486　　Employing the tetrad effect (Masuda and Ikeuchi, 1979) can be useful for understanding the behavior

487　　of REE on water-rock interaction processes. This is based on shale-normalized patterns divided into

four downward convex segments across the entire REE spectrum. A tetrad effect was observed in patterns of the Ln-carbonate complex and REE iron oxyhydroxide complex, represented in samples with pH values ranging between 5.70 and 6.51 (Fig.7). Four upward-curved segments (La-Nd (I), (Pm)-Gd (II), Gd-Ho (III), and Er-Lu (IV)) were observed. These patterns are commonly referred to as the M-type lanthanide tetrad effect (TE) (Masuda et al. 1987; Bau 1996, 1999). The amplitude of the tetrad effect can be used to study the partial dissolution of rock (Bau, 1996, 1999; Irber 1999; Monecke et al. 2002). However, observed M-tetrad effects in Fig.7 were based on modeled complex abundance. It therefore cannot be ruled out that the tetrad effect observed in Fig.7 had been induced by an artifact from speciation modeling. The analytical quality of the data did not allow for quantifying the tetrad effect amplitude with sufficient accuracy. However, the use of the tetrad effect to understand REE behavior through water-rock interactions represents a good perspective for future studies. In particular, the addition of a preconcentration stage will allow for better data accuracy and therefore, better confidence for quantifying the TE, Eu, and Ce anomalies.

Conclusions

A 3 m^3 volume of water saturated with CO_2 was injected into a subsurface fractured aquifer in host rock naturally enriched with trace metals, including REEs. The CO_2-injection into groundwater caused a rapid initial pH decrease (from 7.3 to 5.7), followed by a gradual increase. Chemical changes in the studied system caused by CO_2-injection created significant changes in the geochemical behavior of major elements, trace metals, and dissolved REEs. Enrichment by a factor of nearly four was observed for dissolved REY species. This enrichment was greater for HREE than LREE. The behavior of dissolved REE was evaluated using a geochemical model. Results indicate the main process controlling the release of dissolved REY following CO_2-injection to be the dissolution of iron oxyhydroxides, enhanced by complexation with aqueous carbonate species ($LnCO_3^{2-}$ and $LnCO_3^{-}$). However, the Y/Ho ratio in groundwater suggests that a second source of REEs may have been involved, such as the desorption from carbonate minerals or organic-rich shales.

This study demonstrates the capability of REEs to provide an indication of geochemical interfacial processes occurring at the nanoscale level, during increased interaction between groundwater and host rock, induced by CO_2-injection. This model can help to provide a better understanding of the roles of particle colloids on REEs' mobility in natural systems. These results also present a starting point for evaluation of the environmental impacts of REE exploitation, and for enhancing REE recovery rates using metal oxides under field conditions such as mine drainage. In addition, this study also presents several valuable tools for the understanding of geological fluid-mixing processes, or fluid inclusions formations, which can be useful for understanding deep geological processes.

523

524

525

526

Acknowledgments

Conflict of interest:

The authors declare no conflict of interest.

References:

Alibo, D.S., Nozaki, Y., 1999. Rare earth elements in seawater: particle association, shale-normalization and Ce oxidation. Geochimica et Cosmochimica Acta 63, 363–372.

Bachu S., Bonijoly D., Bradshaw J., Burruss R., Holloway S., Christensen N.P., Mathiassen O.M., 2007. CO2 storage capacity estimation: Methodology and gaps International Journal of Greenhouse Gas Control, Vol. 1, Issue 4, 430-443.

Bachu S., Gunter W.D., Perkins E.H., 1994. Aquifer disposal of CO2: Hydrodynamic and mineral trapping. Energy Conversion and Management. Vol. 35, Issue 4, 269-279

Bau, M. 1991. Rare-earth element mobility during hydrothermal and metamorphic fluid-rock interaction and the significance of the oxidation state of europium. Chemical Geology, Volume 93, 219-230

Bau M., 1996. Controls on the fractionation of isovalent trace elements in magmatic and aqueous systems: evidence from Y/Ho, Zr/Hf, and lanthanide tetrad effect, Contrib Mineral Petrol, 123, 323–333

Bau M., 1999. Scavenging of dissolved yttrium and rare earths by precipitating iron oxyhydroxide: Experimental evidence for Ce oxidation, Y-Ho fractionation, and lanthanide tetrad effect. Geochimica et Cosmochimica Acta, 63, 67–77

Bau M., Alexander B.W., 2009. Distribution of high field strength elements (Y, Zr, REE, Hf, Ta, Th, U) in adjacent magnetite and chert bands and in reference standards FeR-3 and FeR-4 from the Temagami iron-formation, Canada, and the redox level of the Neoarchean ocean. Precambrian Res., 174 (2009), pp. 337-346

Bau M., Koschinsky A., 2009. Oxidative scavenging of cerium on hydrous Fe oxide: Evidence from the distribution of rare earth elements and yttrium between Fe oxides and Mn oxides in hydrogenetic ferromanganese crusts. Geochemical Journal, 43, 37-47,

Bethke, C.M., 2007. Geochemical and Biogeochemical Reaction Modeling, second ed. Cambridge University Press.

Bonnaveira H., Vasseur G., Dufour Y., Vuillemenot P., 1999. Modélisation d'une anomalie géothermique du Lodévois. Comptes Rendus de l'Académie des Sciences - Series IIA - Earth and Planetary Science, Volume 329, Issue 4, 30 August 1999, Pages 251-256,

Brockamp O., Clauer. O., 2013. Hydrothermal and unexpected diagenetic alteration in Permian shales of the Lodève epigenetic U-deposit of southern France, traced by K–Ar illite and K-feldspar dating. Chemical Geology, 357, 18-28

Byrne R. H., and E. R. Sholkovitz, 1996, Chapter 158 Marine chemistry and geochemistry of the lanthanides, in Handbook on the Physics and Chemistry of Rare Earths , edited by K. A. Gschneidner, Jr. and L. Eyring, vol. 23, pp. 497–593, Elsevier Science.

Censi P., Saiano F., Zuddas P., Nicosia A., Mazzola S., Raso M., 2014. Authigenic phase formation and microbial activity control Zr, Hf, and rare earth element distributions in deep-sea brine sediments. Biogeosciences, 11, 1125–1136. doi:10.5194/bg-11-1125-2014

586 Crane R.A., Sapsford D.J., 2018. Sorption and fractionation of rare earth element ions onto nanoscale
587 zerovalent iron particles. Chemical Engineering Journal, 345, 126-137.
588 https://doi.org/10.1016/j.cej.2018.03.148

590 Choi H.S., Yun S.T., Koh Y.K., Mayer B., Park S.S.; Hutcheon I., 2009. Geochemical behavior of rare
591 earth elements during the evolution of CO_2 -rich groundwater: A study from the Kangwon district,
592 South Korea. Chemical Geology, 262, 3, 318-327

594 Chopin C., 2016. Analyse géochimique de la composition des sediments permiens-triasiques du basin
595 de Graissessac-Lodève traçage des sources.
596 http://rgf.brgm.fr/sites/default/files/upload/documents/production-
597 cientifique/Masters/rgf_amipyr2015_ma13_memoire_chopin.pdf

598 Cook, P.J., 2014. Geologically Storing Carbon: Learning from the Otway Project Experience. CSIRO
599 Publishing, Melbourne.

601 Dal Bo F., Hatert F., Baijot M., Philippo S., 2015. Crystal structure of arsenuranospathite from
602 Rabejac, Lode`ve, France. Eur. J. Mineral. 27, 589–597

603 De Carlo, E.H., Wen, X.Y., Irving, M., 1998. The influence of redox reactions on the uptake of
604 dissolved Ce by suspended Fe and Mn oxide particles. Aquat. Geochem. 3, 357–389.

605 Decree S., Pourret O., Baele J.M., 2015. Rare earth element fractionation in heterogenite (CoOOH):
606 Implication for cobalt oxidized ore in the Katanga Copperbelt (Democratic Republic of Congo).
607 Journal of Geochemical Exploration 159:290-301. DOI: 10.1016/j.gexplo.2015.10.005

608 Dulski, P. (1994). Interferences of oxide, hydroxide and chloride analyte species in the determination
609 of rare earth elements in geological samples by inductively coupled plasma‐mass spectrometry.
610 Fresenius' Journal of Analytical Chemistry, 350(4‐5), 194–203. https://doi.org/10.1007/bf00322470

611 European Community, 2010. Critical raw materials for the EU. Report of the Ad-hoc Working Group
612 on defining critical raw materials. Version of 30 July 2010, 84 p.

613 European Commission. (2017). Communication from the commission to the European Parliament,
614 the council, the European economic and social committee and the committee of the regions on the
615 2017 list of Critical Raw Materials for the EU, 8. Retrieved from http://eur-lex.europa.eu/legal-
616 content/EN/TXT/PDF/?uri=CELEX:52017DC0490&from=EN

617 Filho W.L. 2016. An Analysis of the Environmental Impacts of the Exploitation of Rare Earth Metals. In
618 book Rare Earths Industry, chapter 17, 269-277. DOI: 10.1016/B978-0-12-802328-0.00017-6

619 Frei R., Gaucher C., Stolper D., Canfield D.E., 2013. D.E. Fluctuations in late Neoproterozoic
620 atmospheric oxidation — Cr isotope chemostratigraphy and iron speciation of the late Ediacaran
621 lower Arroyo del Soldado Group (Uruguay). Gondwana Res., 23 , pp. 797-811

622 Edahbi M., Plante B., Benzaazaoua M., 2018a. Environmental challenges and identification of the
623 knowledge gaps associated with REE mine wastes management. Journal of Cleaner Production , doi:
624 10.1016/j.jclepro.2018.11.228

625 Edahbi M., Plante B., Benzaazaoua M., Ward M., Pelletier M., 2018b. Mobility of rare earth elements
626 in mine drainage: Influence of iron oxides, carbonates, and phosphates. Chemosphere, 199, 647-654

627 Gal F., Brach M., Braibant G., Bény C., Michel K., 2012. What can be learned from natural
628 analogue studies in view of CO_2 leakage issues in Carbon Capture and Storage
629 applications? Geochemical case study of Sainte-Marguerite area (French Massif
630 Central). International Journal of Greenhouse Gas Control 10, 470-485
631

632 Gilfillan S.M.V, Lollar B.S., Holland G., Blagburn D., Stevens S., Schoell M., Cassidy M., ding Z., Zhou Z.,
633 Lacrampe-Couloume G., Ballentine C.J., 2009. Solubility trapping in formation water as dominant CO_2
634 sink in natural gas fields. Nature. 458, 614–618

635 Haggerty, R., Schroth, M.H., Istok, J.D., 1998. Simplified method of "push–pull" testdata analysis for
636 determining in situ reaction rate coefficients. Ground Water 36(2), 314–324.

637 Haley B. A., Gary P., Klinkhammer G. P., Mc Manus J., 2004. Rare earth elements in pore waters of
638 marine sediments. Geochimica et Cosmochimica Acta, 68, 1265–1279

639 Hannigan R., Sholkovitz E.R., 2001. The development of middle rare earth element enrichments in
640 freshwaters: Weathering of phosphate minerals. Chemical Geology 175(3):495-508

641 Haschkea M., Ahmadianb J., Zeidlera L., Hubrig T., 2016. In-Situ Recovery of Critical Technology.
642 Procedia Engineering. 138, 248 – 257 Elements https://doi.org/10.1016/j.proeng.2016.02.082

643 Humez P., Lagneau V. Lions J., Negrel P., 2013. Assessing the potential consequences of
644 CO_2 leakage to freshwater resources: A batch-reaction experiment towards an isotopic
645 tracing tool. Applied Geochemistry, 30, 178-190

646

647

648 Inguaggiato, C., Censi, P., Zuddas, P., Londono, J.M., Chacon, Z., Alzate, D., Brusca, L., D'Alessandro,
649 W., 2015. Geochemistry of REE, Zr and Hf in a wide range of pH and water composition: the Nevado
650 del   Ruíz   volcano-hydrothermal.   Chem.   Geol.   417,   125–133.
651 http://dx.doi.org/10.1016/j.chemgeo.2015.09.025.

652 Inguaggiato, C., Censi, P., Zuddas, P., Londono, J.M., Chacon, Z., Alzate, D., Brusca, L., D'Alessandro,
653 W. (2016). Zirconium–hafnium and rare earth element signatures discriminating the effect of
654 atmospheric fallout from hydrothermal input in volcanic lake water. Chem. Geol. 433, 1–11.

655 Inguaggiato, C., Garzon, G., Burbano, V., Rouwet, D., 2017. Geochemical processes assessed by Rare
656 Earth Elements fractionation at "Laguna Verde" acidic-sulphate crater lake (Azufral volcano,
657 Colombia). Applied Geochemistry 79:65–74. 10.1016/j.apgeochem.2017.02.013.

658 IPCC, 2005. IPCC Special Report on Carbon Dioxide Capture and Storage. Prepared by Working Group
659 III of the Intergovernmental Panel on Climate Change, Metz, B., O. Davidson, H. C. de Coninck, M.

660 Loos, and L. A. Meyer. Cambridge University Press, Cambridge, United Kingdom and New York, NY,
661 USA, 442 pp.

662 Irber, W., 1999. The lanthanide tetrad effect and its correlation with K/Rb, Eu/Eu∗, Sr/ Eu, Y/Ho, and
663 Zr/Hf of evolving peraluminous granite suites. Geochimica Cosmochimica Acta 63 (3), 489–508.
664

665 Istok, J.D., Humphrey, M.D., Schroth, M.H., Hyman, M.R., O'Reilly, K.T., 1997. Singlewell "push–pull"
666 test for in situ determination of microbial metabolic activities.Ground Water 4, 618–631.

667

668 Johannesson, K.H., Lyons, W.B., Stetzenbach, K.J. and Byrne, R.H., 1995. The solubility control of rare
669 earth elements in natural terrestrial waters and the significance of PO_4^{3-} and CO_3^{2-} in limiting
670 dissolved rare earth concentrations: A review of recent information. Aquat. Geochem. 1, 157-173.

671 Johannesson K.H.,. Stetzenbach K.J.; Hodge V.F., 1997. Rare earth elements as geochemical tracers of
672 regional groundwater mixing. Geochimica et Cosmochimica Acta, 61, 17, 3605-3618
673

674 Jochum KP, Seufert HM, Spettel B, Palme H, 1986. The solar system abundances of Nb, Ta, and Y, and
675 the relative abundances of refractory lithophile elements in differentiated planetary bodies. Geochim
676 Cosmochim Acta 50: 1173–1183

677 Jenkins C., Chadwick A., Hovorka S.D., 2015. The state of the art in monitoring – ten years on.
678 International Journal of Greenhouse Gas Control. 40, 312-349.

679 Keating, E., Fessenden, J., Kanjorski, N., Koning, D., Pawar, R., 2010. The impact of CO_2 on shallow
680 groundwater chemistry: observations at a natural analog site and implications for carbon
681 sequestration. Environ. Earth Sci. 60, 521–536.
682

683 Kharaka Y.K., Cole D.R., Hovorka S.D., Gunter W.D., Knauss K.G., Freifeld B.M., 2006. Gas–water–
684 rock interaction in Frio formation following CO_2 injection: implications for the storage of greenhouse
685 gases in sedimentary basins Geology, 34, 577-580
686

687 Klungness, G.D., Byrne, R.H., 2000. Comparative hydrolysis behavior of the rare earths and yttrium:
688 the influence of temperature and ionic strength. Polyhedron 19, 99–107.
689

690 Laurent D., Lopez M., Chauvet A., Sauvage A.C., Buatier M, Spangenberg J.E., 2017. Sedimentary
691 fluids/fault interaction during syn-rift burial of the Lodeve Permian Basin (Herault, France): An
692 example of seismic-valve mechanism in active extensional faults. Marine and Petroleum Geology 88,
693 303-328
694

695 Lawrence M.G., Greig A., Collerson K.D., Kamber B.S., 2006. Direct quantification of rare earth
696 element concentrations in natural waters by ICP-MS Applied Geochemistry 21, 839–848
697
698

699 Lewis, A.J., Komninou, A., Yardley, B.W., Palmer, M.R., 1998. Rare earth element speciation in
700 geothermal fluids from Yellowstone National Park, Wyoming, USA. Geochim. Cosmochim. Acta 62,
701 657–663.
702

703 Lee, J.H., Byrne, R.H., 1992. Examination of comparative rare earth element complexation behavior
704 using linear free-energy relationships. Geochimica Cosmochimica Acta 56, 1127–1137.
705

Li, C., Liang, H., Wang, S. and Liu, J. (2018) Study of harmful trace elements and rare earth elements in the Permian tectonically deformed coals from Lugou Mine, North China Coal Basin, China. Journal of Geochemical Exploration 190, 10-25.

Little M.G. , Jackson R.B. , 2010. Potential impacts of leakage from deep CO2 geosequestration on overlying freshwater aquifers Environmental Science & Technology, 44, 23, 9225-9232

Liu H., Pourret O., Guo H., Bonhoure J. 2017. Rare earth elements sorption to iron oxyhydroxide: Model development and application to groundwater. Applied Geochemistry, 87, 158-166, https://doi.org/10.1016/j.apgeochem.2017.10.020

Liu F., Lu P., Griffith C., Hedges S.W., Soong Y., Hellevang H., Zhu C., 2012. CO2–brine–caprock interaction: Reactivity experiments on Eau Claire shale and a review of relevant literature. International Journal of Greenhouse Gas Control 7, 153-167

Luo, Y.R., Byrne, R.H., 2001. Yttrium and rare earth element complexation by chloride ions at 25 C. J. Solut. Chem. 30 (9), 837–845.

Luo, Y., Millero, F.J., 2004. Effects of temperature and ionic strength on the stabilities of the first and second fluoride complexes of yttrium and the rare earth elements. Geochimica cosmochimica acta 68 (21), 4301–4308.

Masuda A, Kawakami O, Dohmoto Y, Takenaka T, 1987. Lanthanide tetrad effects in nature: two mutually opposite types, W and M. Geochem J 21: 119–124

McLing T, Smith W, Smith R, 2014. Utilizing Rare Earth Elements as Tracers in High TDS Reservoir Brines in CCS Applications. Energy Procedia 63 (2014) 3963 – 3974

Masuda A. Ikeuchi Y., 1979. Lanthanide tetrad effect observed in marine environment. Geochem. J. 13, 19-22.

Matter, J.M., Takahashi, T., Goldberg, D., 2007. Experimental evaluation of in situ CO2–water–rock reactions during CO2 injection in basaltic rocks: implications for geological CO2 sequestration. Geochemistry, Geophysics, Geosystems 8 (2), 1–19.

Michard, A., 1989. Rare earth element systematics in hydrothermal fluids. Geochim. Cosmochim. Acta 53, 745–750.

Millero, F.J., 1992. Stability constants for the formation of rare earth inorganic complexes as a function of ionic strength. Geochimica Cosmochimica Acta 56, 3123–3132.

Monecke T., Kempe U., Monecke J., Sala M., Wolf D., 2002. Tetrad effect in rare earth element distribution patterns: a method of quantification with application to rock and mineral samples from granite-related rare metal deposits. Geochimica et Cosmochimica Acta, 66,7,1185-1196

Munemoto T., Ohmori K., Teruki I 2015. Rare earth elements (REE) in deep groundwater from granite and fracture-filling calcite in the Tono area, central Japan: Prediction of REE fractionation in paleo- to present-day groundwater, Chemical Geology 417, 58-67

756 Negrel P., Guerrot C. , Cocherie A., Azaroual M. , Brach M. , Fouillac C., 2000. Rare earth elements,
757 neodymium and strontium isotopic systematics in mineral waters: evidence from the Massif Central,
758 France. Applied Geochemistry 15, 1345-1367
759 Noack, C.W., Dzombak, D.A. and Karamalidis, A.K., 2014. Rare earth element distributions and trends
760 in natural waters with a focus on groundwater. Environ. Sci. Technol. 48, 4317-4326.

762 Nordstrom, D.K., Plummer, L.N., Langmuir, D., Busenberg, E., May, H.M., Jones, B.F., Parkhurst, D.L.,
763 1990. Revised Chemical Equilibrium Data for Major Water-mineral Reactions and Their Limitations.

765 Odin B., Conrad G. 1987. Les cinérites, marqueurs asequentiels au sein de la sedimentation
766 permienne, continentale et ryhtmique, du basin de Lodeve (Herault, France). Annales de la Société
767 géologique de Belgique, T.110, 271-278

769 Ohta, A., H. Kagi, M. Nomura, H. Shitsuno, and I. Kawabe, 2009, Coordination study of rare earth
770 elements on Fe oxyhydroxide and Mn dioxides: Part ii. Correspondence of structural change to
771 irregular variations of partitioning coeffcients and tetrad effect variations appearing in interatomic
772 distances, Am. Mineral., 94 (4), 476–486.

773 Ohta A., Kawabe I., 2001. REE(III) adsorption onto Mn dioxide (δ-MnO2) and Fe oxyhydroxide: Ce(III)
774 oxidation by δ-MnO2. Geochimica et Cosmochimica Acta, 65, 5, 695-703

776 Parkhurst, D.L., Appelo, C.A.J., 2013. Description of input and examples for PHREEQC version 3-a
777 computer program for speciation, batch-reaction, one-dimensional transport, and inverse
778 geochemical calculations. U. S. Geol. Surv. Tech. methods, book 6, 497.

779 Pérez-López R. , Delgado J., Nieto J.M., Márquez-García B.(2010). Rare earth element geochemistry of
780 sulphide weathering in the São Domingos mine area (Iberian Pyrite Belt): a proxy for fluid–rock
781 interaction and ancient mining pollution. Chem. Geol., 276, 29-40

782 Pearce J.K, Kirste D.M., Dawson G.K.W. ; Farquhar S.M., Biddle D., Golding S.D., Rudolph V., 2015.
783 SO2 impurity impacts on experimental and simulated CO2–water–reservoir rock reactions at carbon
784 storage conditions. Chemical Geology,399, 65-86

786 Perry E. P., Gysi A.P., 2018. Rare Earth Elements in Mineral Deposits: Speciation in Hydrothermal
787 Fluids and Partitioning in Calcite. Geofluids Volume 2018, Article ID 5382480, 19 pages
788 https://doi.org/10.1155/2018/5382480Pourret, O., Davranche, M., Gruau, G., Dia, A., 2007a. Rare
789 earth elements complexation with humic acid. Chem. Geol. 243, 128–141.

790 Pourret O., Dia A., Davranche M., Gruau G., Hcheel. 24Ang,e M.,2007b. Organo-colloidal control on
791 major- and trace-element partitioning in shallow groundwaters: Confronting ultrafiltration and
792 modelling. Applied Geochemistry 22 (2007) 1568ellin
793 Pourret, O., Martinez, R.E., 2009. Modeling lanthanide series binding sites on humic acid. J. colloid
794 interface Sci. 330 (1), 45–50.

795 Pourret, O., Gruau, G., Dia, A., Davranche, M., Molenat, J., 2010. Colloidal control on the distribution
796 of rare earth elements in shallow groundwaters. Aquat. Geochem. 16 (1), 31.

797 Pourret O., Tuduri J. 2017. Continental shelves as potential resource of rare earth elements, Scientific
798 Reports, 7 :5857

799 Qu, C. L., Liu, G., and Zhao, Y. F. 2009. Experimental study on thefractionation of yttrium from holmium
800 during the coprecipita-tion with calcium carbonates in seawater solutions, Geochem. J., 43, 403–414

801

802 Quinn, K.A., Byrne, R.H., Schijf, J., 2006. Sorption of yttrium and rare earth elements by amorphous
803 ferric hydroxide: influence of solution complexation with carbonate. Geochimica Cosmochimica Acta
804 70 (16), 4151–4165

805 Quinn, K.A., Byrne, R.H., Schijf, J., 2007. Sorption of yttrium and rare earth elements by amorphous
806 ferric hydroxide: influence of temperature. Environ. Sci. Technol. 41 (2), 541–546.

807 Rillard, J., Gombert, P., Toulhoat, P., Zuddas, P., 2014. Geochemical assessment of CO2 perturbation
808 in a shallow aquifer evaluated by a push–pull field experiment. International Journal of Greenhouse
809 Gas Control 21, 23–32.

810 Shabani M.B., Akagi T., Masuda A., 1992. Preconcentration of trace rare-earth elements in seamater
811 by complexation with bis(2-ethylhexyl) hydrogen phosphate adsorbed on a C18 cartridge and
812 determination by inductively coupled plasma mass spectrometry. Analytical Chemistry, 64(7), 737-
813 743

814 Shand P., Johannesson K.H., Chudaev O. V., Chudaeva V. , Edmunds W. M., 2005. Rare Earth Element
815 Contents of High pCO2 Groundwaters of Primorye, Russia: Mineral Stability and complexation
816 Controls. In book: Rare Earth Elements in Groundwater Flow Systems, DOI: 10.1007/1-4020-3234-
817 X_7

818 Shannon, R.T., 1976. Revised effective ionic radii and systematic studies of interatomic distances in
819 halides and chalcogenides. Acta Crystallogr. Sect. A Cryst. Phys. Diffr. Theor. general Crystallogr. 32
820 (5), 751–767.Schijf, J., Marshall, K.S., 2011. YREE sorption on hydrous ferric oxide in 0.5 M NaCl
821 solutions: a model extension. Mar. Chem. 123 (1), 32–43.

822
823   Schijf, J., Byrne, R.H., 2004. Determination of SO4 β1 for yttrium and the rare earth elements at
824 I=0.66 m and t=25 ºC-implications for YREE solution speciation in sulfate-rich waters. Geochimica
825 cosmochimica acta 68 (13), 2825–2837.

826 Sholkovitz, E. R., 1995, The aquatic chemistry of rare earth elements in rivers and estuaries, Aquat.
827 Geochem.,1(1), 1–34

828 Shu X., , Liu Y., 2019. Fluid inclusion constraints on the hydrothermal evolution of the Dalucao
829 Carbonatite-related REE deposit, Sichuan Province, China. Ore Geology Reviews 107, 41–57

830
831 Siirila, E.R., Navarre-Sitchier, A., Maxwell, R.M., McCray, J.E., 2012. A quantitative methodology to

832 assess the risks to human health from CO2 leakage into groundwater, Advances Water Resources 36,

833 146-164.

834 Steinmann, M. and Stille, P., 2008. Controls on transport and fractionation of the rare earth elements
835 in stream water of a mixed basaltic-granitic catchment (Massif Central, France). Chem. Geol. 254, 1-
836 18.

837 Takahashi Y., Yoshida H., Sato N., Hama K., Yusa Y., Shimizu H., 2002. W- and M-type tetrad effects in
838 REE patterns for water–rock systems in the Tono uranium deposit, central Japan. Chemical Geology
839 184, 311 – 335

840 Takahashi Y., Yamamoto M., Yamamoto Y., Tanaka K. 2010. EXAFS study on the cause of enrichment
841 of heavy REEs on bacterial cell surfaces. Geochimica et Cosmochimica Acta 74,5443–5462

842

843 Tang, J., Johannesson, K.H., 2003. Speciation of rare earth elements in natural terrestrial waters:
844 assessing the role of dissolved organic matter from the modeling approach. Geochimica
845 Cosmochimica Acta 67 (13), 2321–2339.

846 Tostevin, R., Shields, G. A., Tarbuck, G. M., He, T., Clarkson, M. O., & Wood, R. A. (2016). Effective use
847 of cerium anomalies as a redox proxy in carbonate-dominated marine settings. Chemical Geology,
848 438, 146-162.

849 Vahidi E., Navarro J., Zhao F., 2016. An initial life cycle assessment of rare earth oxides production
850 from ion-adsorption clays. Resources, Conservation and Recycling. 113, 1–11

851 Verplanck, P.L., Nordstrom, D.K., Taylor, H.E., Kimball, B.A., 2004. Rare earth element partitioning
852 between iron oxyhydroxides and acid mine waters. Appl. Geochem. 19, 1339–1354.

853 Wilkin, R.T., Digiulio, D.C., 2010. Geochemical impacts to groundwater from geologic carbon

854 sequestration: controls on pH and inorganic carbon concentrations from reaction path and kinetic

855 modeling. Environmental Science & Technology 44, 4821-4827.

856 Wood, S.A., 1990. The aqueous geochemistry of the rare-earth elements and yttrium: 1. Review of
857 available low-temperature data for inorganic complexes and the inorganic REE speciation of natural
858 waters. Chem. Geol. 82, 159–186.

859 Worrall, F. and Pearson, D.G. (2001) Water-rock interaction in an acidic mine discharge as indicated
860 by rare earth element patterns. Geochim. Cosmochim. Acta 65, 3027-3040.

861 Wunsch, A., Navarre-Sitchler, A.K., Moore, J., Ricko, A., McCray, J.E., 2013. Metal release from

862 dolomites at high partial-pressures of CO2. Applied Geochemistry 38, 33–47.

863

864 Yang, J., Verba, C., Torres, M., Hakala, J.A., Empirically assessing the potential release of rare earth
865 elements from black shale under simulated hydraulic fracturing conditions, Journal of Natural Gas
866 Science & Engineering (2018), doi: 10.1016/j.jngse.2017.09.011.
867

868 Zwahlen C.. , Cathy Hollis C. , Lawson M., Becker S.P., Boyce A., Zhou Z., Holland G. (2019).
869 Constraining the fluid history of a CO2‐H2S reservoir: Insights from stable isotopes, REE, and fluid
870 inclusion microthermometry. Geochemistry, Geophysics, Geosystems, 20, 359–382.
871 https://doi.org/10.1029/ 2018GC007900
872 .

873
874

875

876

877
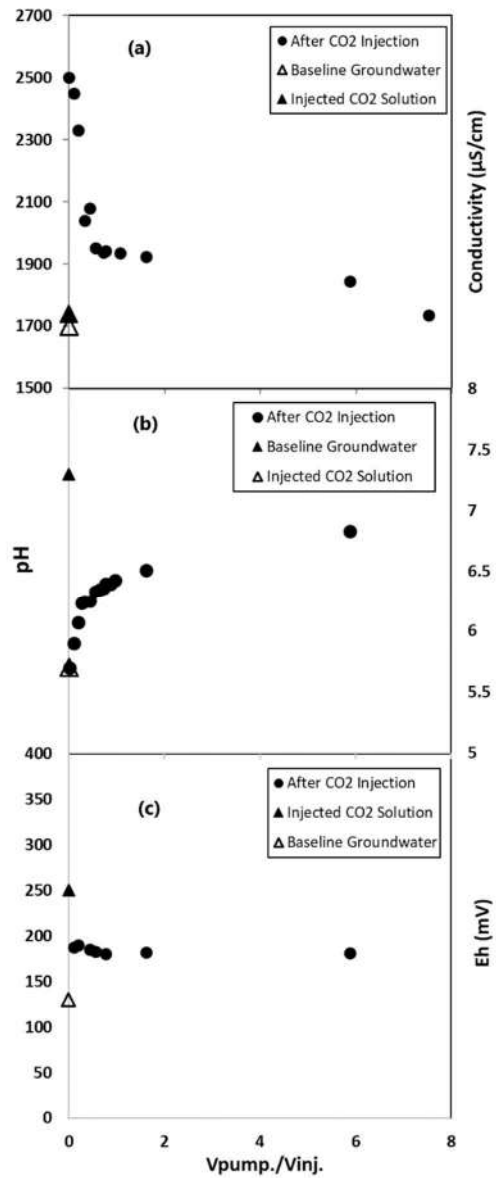
Fig. 1: (a) Conductivity (µS/cm) of groundwater as a function of a function of the ratio pumped (Vp.) volume to injection volume (Vinj.). Values are indicated for baseline groundwater, injected CO_2 solution and groundwater re-pumped after CO_2 injection; (b) pH values as a function of ratio Vp./Vinj.; (c) Redox potential (Eh in mV) measured as a function of ratio Vp./Vinj.
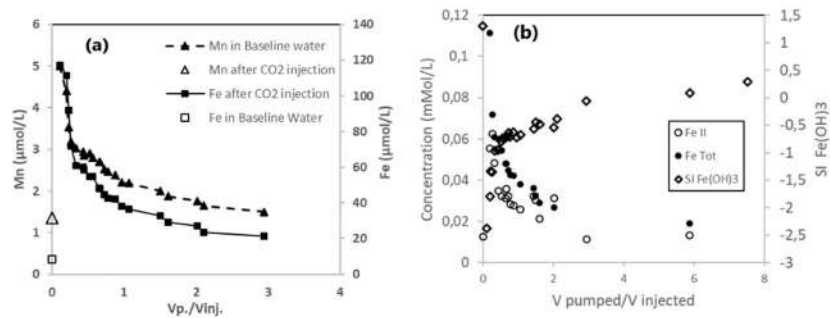
Fig. 2 : (a) Molar concentration (µmol/L) of dissolved iron (Fe, right axis) and manganese (Mn, left axis) as a function of the ratio pumped volume (Vp.) to injection volume (Vinj.);(b) Molar concentration (mMol/L) of total dissolved iron (Fe Tot, left axis), iron two Fe2+ (Fe II) and Saturation Index in Ferrihydrite Fe(OH)3 (left axis)as a function of ratio Vp./Vinj. Figure (b) is from Rillard et al 2014.
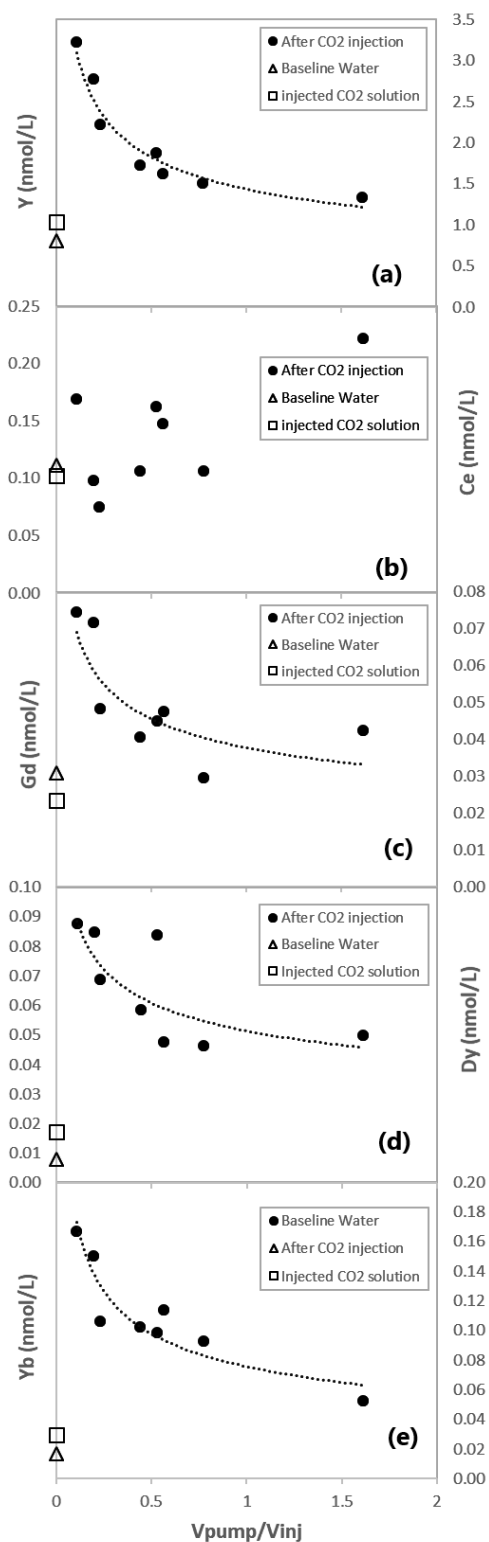
Fig. 3: (a) Molar concentration (nmol/L) in yttrium as function of the ratio pumped volume (Vp.) to injection volume (Vinj.), representative of HREE group; (b) Cerium concentration as a function of Vp./Vinj. ratio, representative of LREE group; (c) Gadolinium concentration (nmol/L) as a function of ratio Vp./Vinj. representative of MREE group; (d) Dysprosium concentration (nmol/L) as a function of

ratio Vp./Vinj. representative of MREE group; (e) Ytterbium concentration (nmol/L) as function of ratio Vp./Vinj. representative of HREE group.
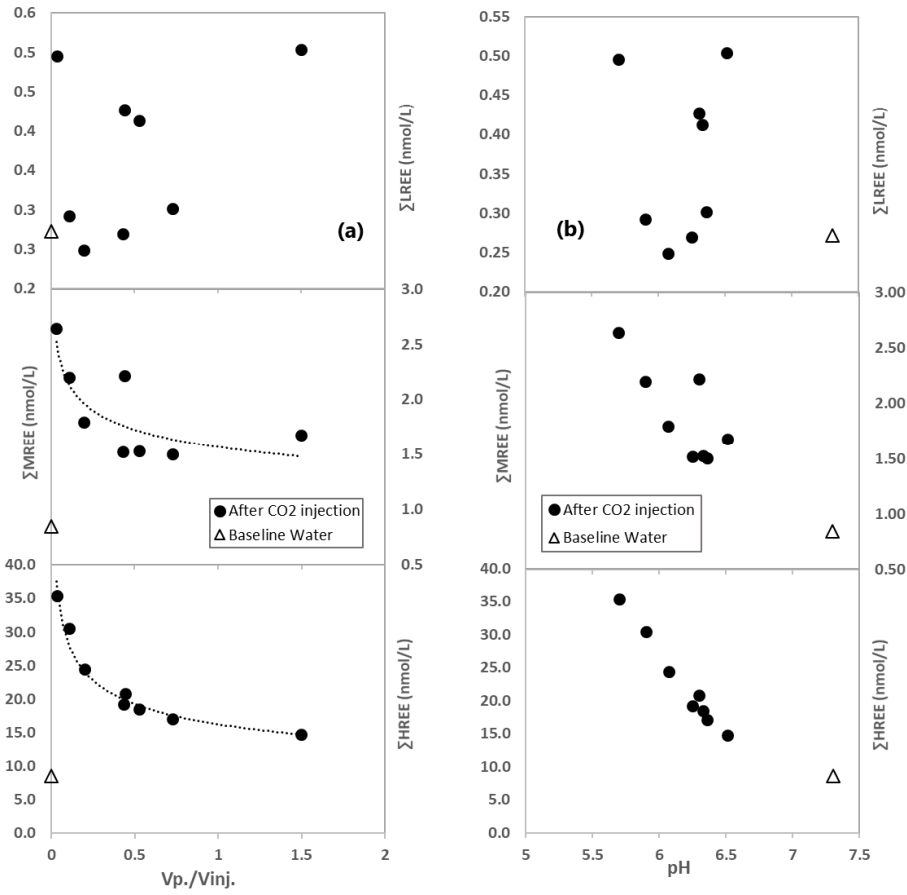
Fig. 4 : (a) Sum of LREE (La, Ce, Pr, Sm), MREE (Eu, Gd, Tb, Dy, Ho), HREE (Er, Tm, Yb, Lu, Y) as function of the ratio pumped volume (Vp.) to injection volume (Vinj.) ; (b) Sum of LREE (La, Ce, Pr, Sm), MREE (Eu, Gd, Tb, Dy, Ho), HREE (Er, Tm, Yb, Lu, Y) as function of pH
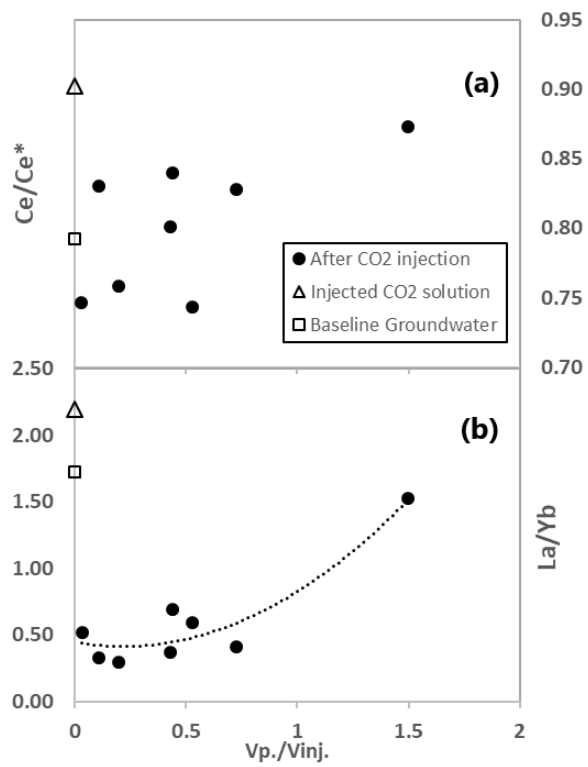
Fig. 5 : (a) Cerium anomaly Ce/Ce* as a function of the ratio pumped volume (Vp.) to injection volume (Vinj.); (b) La/Yb ration as a function of the ratio pumped volume (Vp.) to injection volume (Vinj.)
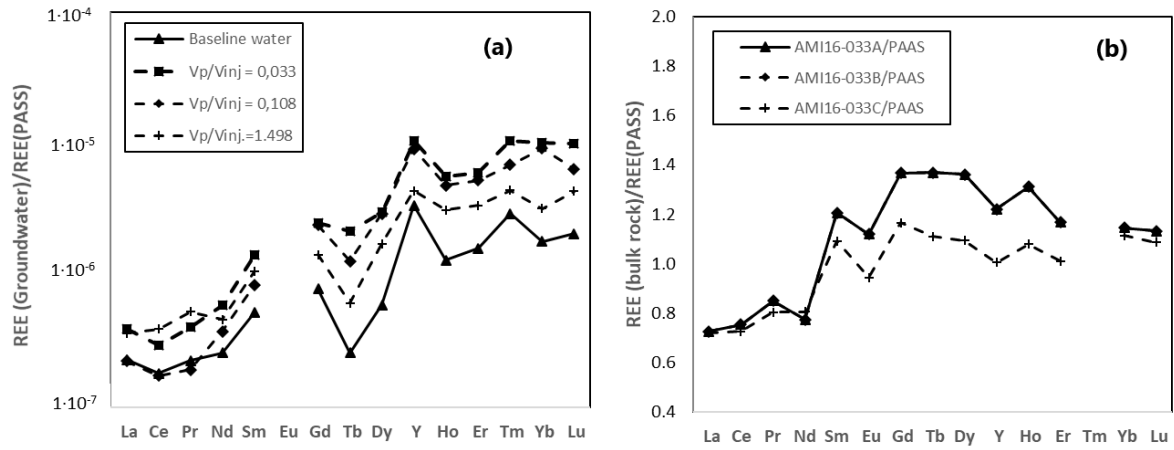
Fig. 6: (a) Dissolved REE concentrations in groundwater samples normalized to Post Archean Australian Shale (PAAS), four representative samples are illusatrated (baseline groundwater, Vp/Vinj. = 0.033, Vp/Vinj=0.108, Vp/Vinj=1.498); (b) REE concentrations in bulk rock samples normalized to Post Archean Australian Shale (PAAS), data issued from Chopin (2016).
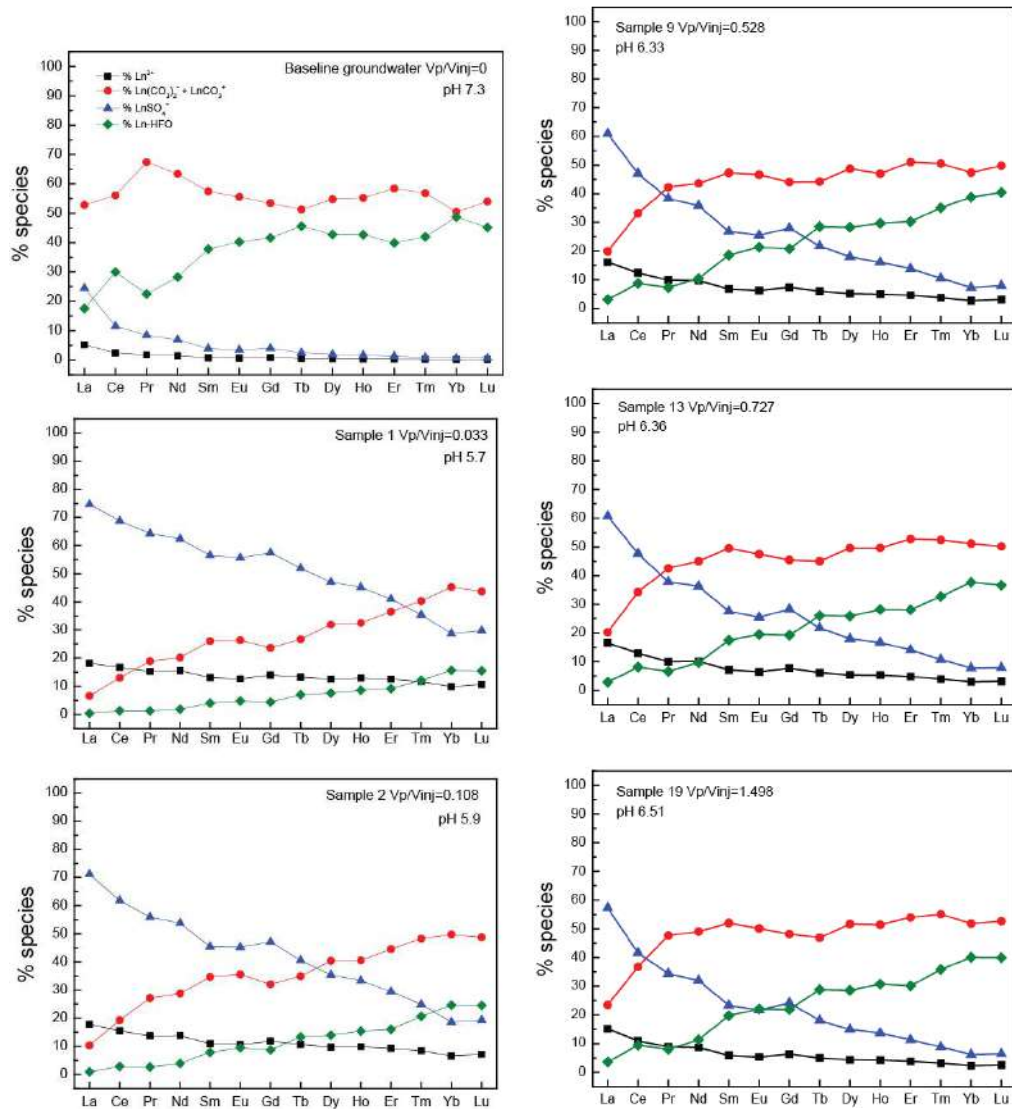
Fig. 7 : Proportion (%) of Ln-Carbonate, Ln-Sulphate, Ln-iron oxihydroxide complex and free Ln^{3+} calculated by the geochemical model in sample Baseline Water, and selected samples following CO_2 injection (Sample 1, Sample 2, Sample 9 , Sample 13, Sample 19). The pH values and Vp/Vinj ratio of each individual sample are indicated in the diagrams.
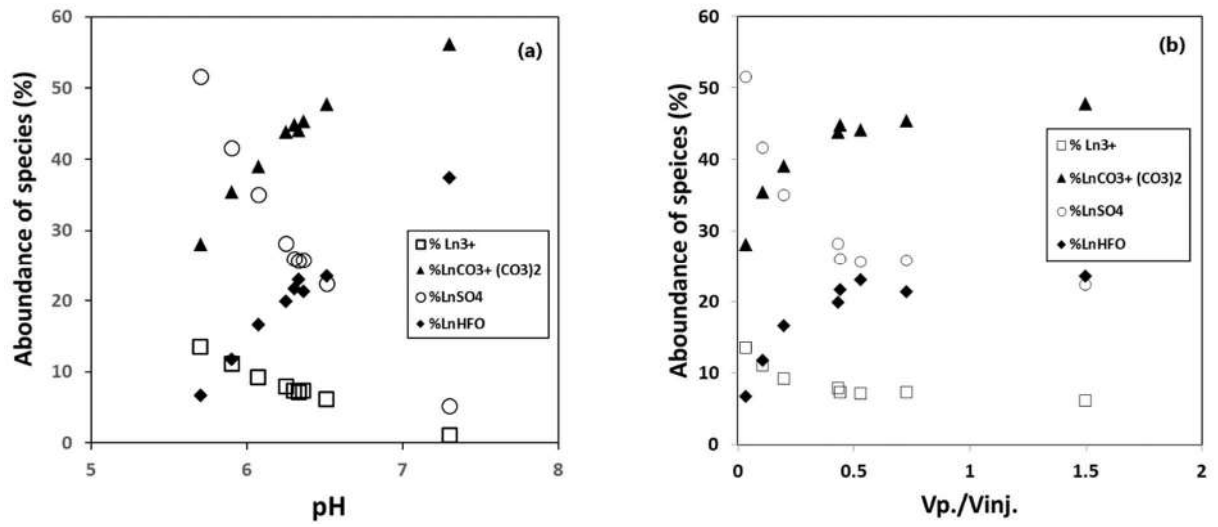
Fig.8: Total proportion (%) of Ln-Carbonate, Ln-Sulphate, Ln-iron oxihydroxide complex and free Ln^{3+} calculated by the geochemical model as a function of (a) pH and (b) the ratio pumped volume (Vp.) to injection volume (Vinj.)
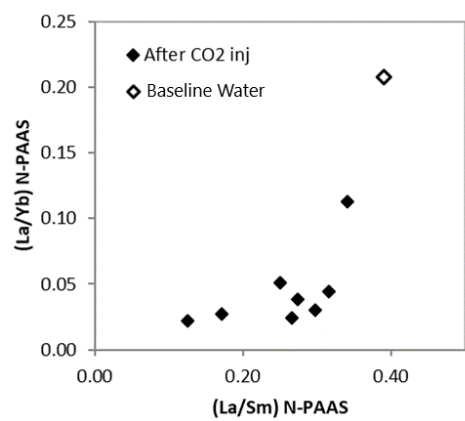
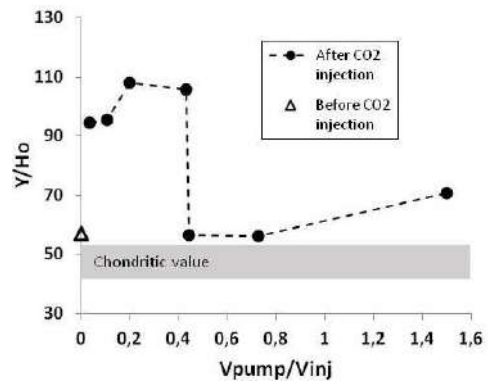Fig. 9: La/Yd ratio as a function of La/Sm ratio (normalized to PAAS)

Fig.10: Y/Ho molar ratio as a function of Vpump./Vinj. ratio. Groundwater composition before CO_2 injection is represented by white triangle.
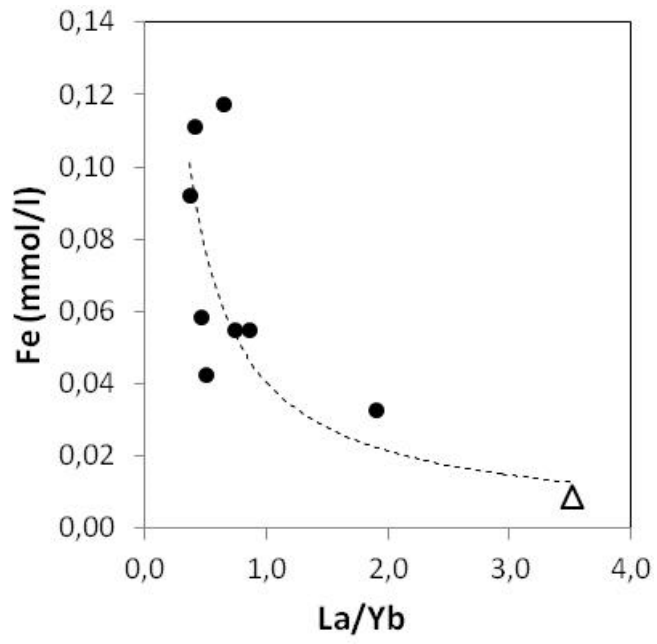
Fig.11: Molar concentration in dissolved iron (mmol/l) as a function of La/Yb ratio. Groundwater composition before CO_2 injection is represented by white triangle.

Table Caption:

Table 1 : List of studied samples. The corresponding ratio of pumped on injected volume ("V pump./V inj.") and the field measured pH, redox Eh (mV) and conductivity (μS/cm) for each sample are reported. The sample "Baseline Water" corresponds to the baseline water before CO_2 saturation and the sample "Injected CO2 Solution" corresponds to the baseline water saturated with CO_2 and injected for the experiment.

Sample	V pump./V inj.	pH	Eh (mV)	Conductivity (μS/cm)
Baseline Water	0	7,3	130	1697
Injected CO2 Solution	0	5,7	250	1736
Sample 1	0,033	5,7	187,3	2500
Sample 2	0,108	5,9	189,6	2450
Sample 3	0,198	6,07	185,4	2330
Sample 7	0,432	6,25	183,1	2080
Sample 8	0,442	6,3	181,2	2040
Sample 9	0,528	6,33	180,7	1951
Sample 13	0,727	6,36	182,4	1938
Sample 19	1,498	6,51	180,9	1923